RSC Advances

PAPER

View Article Online
View Journal | View Issue

Cite this: *RSC Adv.*, 2020, **10**, 18377

Facet-, composition- and wavelength-dependent photocatalysis of Ag_2MoO_4†

Lucas Warmuth, Christian Ritschel and Claus Feldmann *

Received 1st April 2020
Accepted 7th May 2020

DOI: 10.1039/d0ra02953j

rsc.li/rsc-advances

Faceted β-Ag_2MoO_4 microcrystals are prepared by controlled nucleation and growth in diethylene glycol (DEG) or dimethylsulfoxide (DMSO). Both serve as solvents for the liquid-phase synthesis and surface-active agents for the formation of faceted microcrystals. Due to its reducing properties, truncated β-Ag_2MoO_4@Ag octahedra are obtained in DEG. The synthesis in DMSO allows avoiding the formation of elemental silver and results in β-Ag_2MoO_4 cubes and cuboctahedra. Due to its band gap of 3.2 eV, photocatalytic activation of β-Ag_2MoO_4 is only possible under UV-light. To enable β-Ag_2MoO_4 for absorption of visible light, silver-coated β-Ag_2MoO_4@Ag and $Ag_2(Mo_{0.95}Cr_{0.05})O_4$ with partial substitution of $[MoO_4]^{2-}$ by $[CrO_4]^{2-}$ were prepared, too. The photocatalytic activity of all the faceted microcrystals (truncated octahedra, cubes, cuboctahedra) and compositions (β-Ag_2MoO_4, β-Ag_2MoO_4@Ag, β-$Ag_2(Mo_{0.95}Cr_{0.05})O_4$) is compared with regard to the photocatalytic decomposition of rhodamine B and the influence of the respective faceting, composition and wavelength.

Introduction

Nanosized molybdenum and tungsten oxides have proven to be interesting with regard to a wide range of properties, including catalysis, applicability in high-power batteries and sensing, and luminescence.[1] Beside the binary MoO_3 and WO_3,[2] ternary molybdate and tungstate phases are intensely studied as well (*e.g.*, $CaWO_4$, $CdMoO_4$, $CoMoO_4$).[3] With regard to their properties, photocatalysis can be considered as particularly important. Special attention has been recently paid to molybdates/tungstates with closed-shell and lone-pair containing metal cations like Pb(II), Sn(II) or Bi(III) due to their unique electronic and structural features mediated by the "non-bonding" electron pairs.[3f,4] In this regard, especially, bismuth molybdate and bismuth tungstate have been intensely studied.[5] For efficient photocatalysis, moreover, faceted microcrystals have turned out to be most promising.[6]

Aiming at molybdates/tungstates with closed-shell cations, silver molybdate has been also classified to be an catalytically interesting material.[7] The cubic β-Ag_2MoO_4 exhibits a direct band gap of 3.2 eV,[8] which is too high in energy for visible-light activation, whereas a band gap of 1.26 eV was reported for the tetragonal α-Ag_2MoO_4 phase.[9] However, α-Ag_2MoO_4 is metastable and was yet only described twice as a nanomaterial.[9,10] The thermodynamically most stable β-Ag_2MoO_4 is already available with different morphologies, including spheres, rods, cylinders as well as octahedra and cube-like shapes.[11] To this concern, microemulsions,[11b] hydrothermal and solvothermal synthesis were applied with water, methanol or ethanol heated in autoclaves up to temperatures of 180 °C.[8,11a,c–e] Shape control and formation of specific facets were predominately initiated by high-molecular-weight surface-active agents like as polyvinylpyrrolidone (PVP) or 2,3-bis(2-pyridyl)pyrazine (BPP).[10,11a,c–e] Despite of successful shape control, such high-molecular-weight stabilizers suffer from the necessity of their removal after the synthesis, since the photocatalytically active surface is otherwise blocked by the stabilizer. Motivated by the great interest in photocatalytic nanomaterials, we have already studied niobates, molybdates and tungstates such as Au@Nb@$H_xK_{1-x}NbO_3$ nanopeapods,[12] $CuMoO_4$ nanoparticles,[13] or faceted β-$SnWO_4$.[14] In this study, we report on a controlled liquid-phase synthesis of faceted β-Ag_2MoO_4 microcrystals, the chromate-driven red-shift of the light absorption as well as on the facet-, composition- and wavelength-depending photocatalysis.

Experimental

Material synthesis

General aspects. Silver nitrate ($AgNO_3$, p.a., VWR), potassium molybdate (K_2MoO_4, 98%, ABCR), potassium chromate (K_2CrO_4, 99%, ABCR), diethylene glycol (DEG, $C_4H_{10}O_3$, 99%, Alfa Aesar) and dimethylsulfoxide (DMSO, C_2H_6OS, 99.5%, Sigma-Aldrich) were used as purchased. Zwitterionic rhodamine B (RhB, $C_{28}H_{31}ClN_2O_3$, 99%, Acros Organics) was used as model dye for photocatalytic dye degradation without further purification.

Institut für Anorganische Chemie, Karlsruhe Institute of Technology (KIT), Engesserstraße 15, D-76131 Karlsruhe, Germany. E-mail: claus.feldmann@kit.edu; Tel: +49-721-60842855

† Electronic supplementary information (ESI) available: Data related to photoluminescence and shape of catalyst before and after photocatalysis. See DOI: 10.1039/d0ra02953j

DEG-/DMSO-mediated synthesis of β-Ag_2MoO_4 microcrystals. K_2MoO_4 (0.5 mmol) was dissolved in 50 mL of the liquid phase (DEG or DMSO/H_2O, Table 1). In the case of chromate substitution, 0.025 mmol of K_2MoO_4 were exchanged by K_2CrO_4. After dissolution of K_2MoO_4, an aqueous solution of 1 mmol of $AgNO_3$ in 2 mL of deionized water was injected into the molybdate solution. The temperature of injection was adjusted to 0, 50 or 80 °C (Table 1) with an ice bath or a heating mantle. Subsequent to $AgNO_3$ injection, a suspension was instantaneously obtained and allowed to come to room temperature within 1.0 or 2.5 hours (Table 1). For the heated samples, the round-bottomed flask was left inside the heating mantle for slow cooling (2.5 hours), whereas the flask was immediately removed from the heating mantle for fast cooling (1.0 hours). The resulting suspensions were centrifuged and the solid purified by repeated resuspension and centrifugation in/from water, which was performed three times. Finally, the β-Ag_2MoO_4 samples were dried at room temperature.

Analytical methods

Field emission scanning electron microscopy (FESEM, Zeiss Supra 40VP equipped with energy dispersive X-ray spectrometer, EDXS) was used to determine the morphology of the as-prepared faceted β-Ag_2MoO_4 microcrystals. The microcrystals were suspended in ethanol, dropped and dried on sliced pieces of a silicon wafer (5 × 5 mm).

Crystallinity and chemical composition of the faceted β-Ag_2MoO_4 microcrystals were examined by XRD (Stoe STADI-MP diffractometer, equipped with Ge-monochromator and Cu-$K_{\alpha1}$ radiation, 40 kV, 40 mA). About 10 mg of the microcrystals were deposited onto acetate foil and fixed with scotch tape.

To determine the zeta potential of microcrystal β-Ag_2MoO_4 suspensions, a Zetasizer Nano ZS from Malvern Instruments was used. About 1 mg of the microcrystals was suspended in water and ultrasonicated for 5 min prior to the analysis.

UV-Vis spectra of β-Ag_2MoO_4 microcrystals were recorded on a UV 2700 spectrometer (Shimadzu). 4–8 mg of the microcrystals were mixed with 100–120 mg of dried $BaSO_4$ (spectroscopic grade) and measured against dried $BaSO_4$ as a reference. The determination of the band gap was conducted based on the Kubelka–Munk formalism and Tauc plots.

Fourier-transform infrared (FT-IR) spectroscopy was performed with a Bruker Vertex 70 FT IR spectrometer. To this concern, the microcrystals were grounded with dried KBr (1–2 mg with 400 mg KBr) and pressed for 15 min under 50 kN.

Volumetric nitrogen sorption measurements (BEL BELSORP-max) were carried out at 77 K with nitrogen as analyte. According to the BET formalism (BET: Brunauer–Emmett–Teller) the specific surface area was deduced. Prior to the analysis, the microcrystalline samples were dried at 120 °C in vacuum.

Photocatalytic measurements

The photocatalytic dye degradation was performed with a Shimadzu Excalibur measuring head linked to the aforementioned UV-Vis spectrometer. For measurement, the quartz flask contained an aqueous suspension of the respective faceted β-Ag_2MoO_4 microcrystals (20 mg in 110 mL; 0.18 g L^{-1}) and RhB (0.20 mg L^{-1}). This suspension was continuously mixed with a magnetic stirrer. For photocatalytic degradation, a LOT Class ABA solar simulator (type LS0805) was applied that emits a spectrum of AM 1.5 G solar light (100 mW cm^{-2}). Beside illumination with simulated sunlight, cut-off filters (Horiba, <350 nm and <400 nm) were applied to cut-off UV or UV and blue light. Prior to illumination, the suspensions were magnetically stirred in the dark for 1 h to ensure homogenous distribution of the photocatalyst and the dye. All experiments were carried out at room temperature and in air. The course of the RhB degradation was continuously monitored by comparing the intensity of the strongest dye absorption ($\lambda_{RhB} = 554$ nm) with the initial absorption at the beginning of the experiment. The obtained transmission-time plots were fitted by linear or allometric fits. For reasons of clarity, only every tenth raw data point is shown.

Results and discussion

Morphology control

Based on our knowhow on the synthesis of molybdate and tungstate nanoparticles in high-boiling alcohols (so-called

Table 1 Parameter of synthesis to obtain faceted β-Ag_2MoO_4 microcrystals

				Composition
Morphology	Type of solvent	Temperature of injection/°C	Time of cooling/h	Sample color
Spheres	DEG	80	1.0	β-Ag_2MoO_4@Ag Greyish
Truncated octahedra	DEG	80	2.5	β-Ag_2MoO_4@Ag Greyish
Spheres	DMSO/H_2O 20 : 80 to 80 : 20	0–80	1.0–2.5	β-Ag_2MoO_4 Colorless
Cubes	DMSO/H_2O 85 : 15	0	2.5	β-Ag_2MoO_4 Colorless
Cuboctahedra	DMSO/H_2O 85 : 15	50	2.5	β-Ag_2MoO_4 Colorless
Cuboctahedra	DMSO/H_2O 85 : 15	50	2.5	$Ag_2(Mo_{0.95}Cr_{0.05})O_4$ Yellow

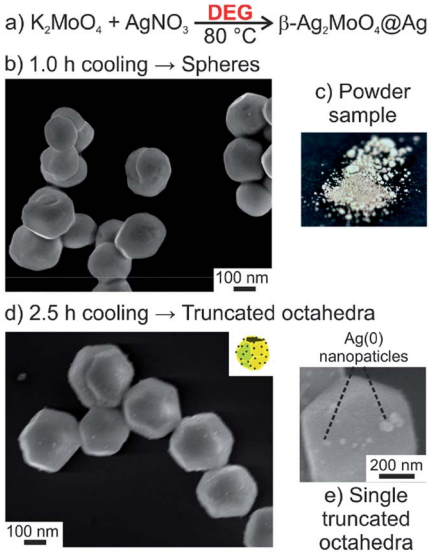

Fig. 1 Synthesis of β-Ag_2MoO_4@Ag in diethylene glycol (DEG): (a) scheme of synthesis; (b) SEM image of microspheres after fast cooling; (c) photo of powder sample; (d) SEM image of truncated octahedra after slow cooling with surface-allocated Ag(0) nanoparticles stemming from DEG-driven reduction; (e) selected truncated octahedron with silver spots.

polyol synthesis)[13,15] and the realization of faceted microcrystals of β-$SnWO_4$,[14] we have tried to prepare Ag_2MoO_4 nanoparticles *via* a polyol-mediated approach. For this purpose, diethylene glycol (DEG) was chosen (Fig. 1a). In general, the advantage of DEG as a water-comparable but high-boiling solvent relates to its moderately coordinating properties, so that additional high-molecular-weight surface-active agents are not required. K_2MoO_4 was selected as starting material containing the required tetrahedral $[MoO_4]^{2-}$ anion. Here, it needs to be noticed that starting materials containing octahedral (MoO_6) building units (*e.g.* $(NH_4)_6Mo_7O_{24}$) show inappropriate solubility and often result in incomplete reactions with several by-products.

For the synthesis, a concentrated aqueous solution of $AgNO_3$ was injected at a temperature high enough for the crystallization of β-Ag_2MoO_4 (≥80 °C) but low enough to avoid instantaneous DEG-driven reduction of Ag^+ (<100 °C) (Table 1, compare Fig. 5a). Fast cooling (1.0 hour) indeed results in highly crystalline β-Ag_2MoO_4 but predominately yields non-faceted, spherical particles with diameters of 200–300 nm (Fig. 1b). Slow cooling (2.5 hours), in contrast, supports facet formation and results in truncated β-Ag_2MoO_4 octahedra with edge lengths of 100 nm (Fig. 1d). For both the spherical particles and the truncated octahedra, however, certain formation of silver could not be avoided. Its formation is qualitatively indicated by the greyish color of the samples (Fig. 1c) and can be quantified by UV-Vis spectra displaying the characteristic plasmon-resonance absorption of nanosized silver (Table 1, compare Fig. 5b).[16] Moreover, silver nanoparticles, 32 ± 13 nm in diameter, are clearly visible on SEM images as bright spots on the surface of the β-Ag_2MoO_4 microcrystals (Fig. 1e). Since visible light could be absorbed *via* the plasmon-resonance absorption, these Ag(0) nanoparticle-coated β-Ag_2MoO_4 microcrystals (Ag_2MoO_4@Ag) nevertheless be relevant for photocatalysis.

Aiming at pure, faceted β-Ag_2MoO_4 microcrystals without elemental silver, we have modified the synthesis. In order to maintain the polarity of the solvent in regard of the solubility of the starting materials but to avoid the reducing properties of DEG, we have selected a mixture of dimethylsulfoxide (DMSO) and water as alternative liquid phase (Fig. 2a). Highly crystalline β-Ag_2MoO_4 was indeed obtained upon injection of aqueous $AgNO_3$ into a solution of $KMoO_4$ in DMSO/water at a temperature of 0 to 50 °C (Table 1). The shape of the resulting Ag_2MoO_4 turned out to be highly dependent on the DMSO : water ratio. Thus, more-or-less spherical microcrystals were formed at high water contents (Table 1, Fig. 2b and c). Optimal conditions for the formation of well-faceted microcrystals including cuboctahedra and cubes were observed for a DMSO : H_2O ratio of 85 : 15 (Table 1 and Fig. 2d). In addition to the formation of specific crystal facets, the size of the microcrystals was significantly reduced from >5 μm to 1–2 μm upon decreasing the amount of water (Fig. 2d). The water content is limited to a minimum of 15% due to the poor solubility of K_2MoO_4. Finally, it should be noticed that the formation of elemental silver was prevented with these experimental conditions of the DMSO-mediated synthesis. Thus, the β-Ag_2MoO_4 microcrystals are colorless and do not show any plasmon-resonance absorption (Table 1 and Fig. 2e, compare Fig. 5b). They also do not show Ag(0)-related spots on electron-microscopy images (Fig. 2b–d). Small Ag(0)-related spots only appear on electron-microscopy images after certain period of exposition under the electron beam (compare Fig. 4).

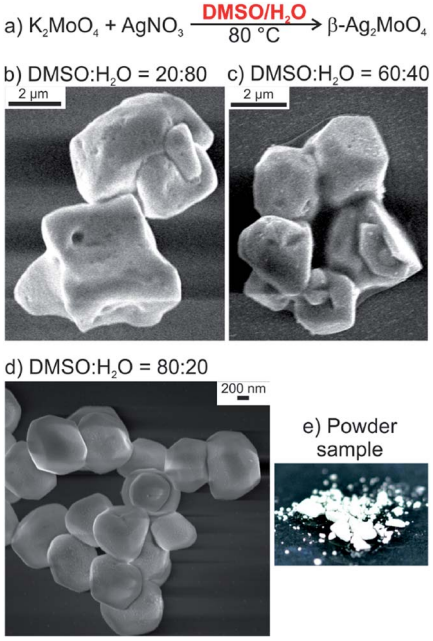

Fig. 2 Synthesis of β-Ag_2MoO_4 in dimethylsulfoxide (DMSO): (a) scheme of synthesis; (b–d) SEM images of microparticles obtained at different DMSO : H_2O ratios. Spots of Ag(0) arise due to electron-beam irradiation; (e) photo of powder sample.

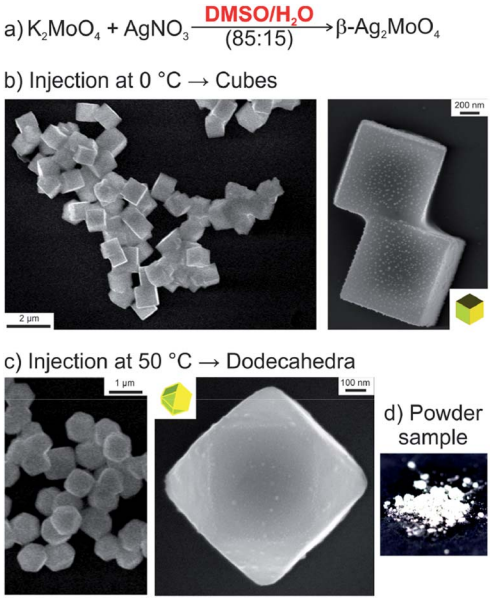

Fig. 3 Synthesis of faceted β-Ag_2MoO_4 in dimethylsulfoxide (DMSO): (a) scheme of synthesis; (b) SEM image of cubes after $AgNO_3$ injection at 0 °C; (c) SEM image of cuboctahedra after $AgNO_3$ injection at 50 °C (both with DMSO : H_2O = 85 : 15). Spots of Ag(0) arise under irradiation with the electron beam; (d) photo of powder sample.

To obtain cuboctahedra and cubes – beside the aforementioned water content – the temperature for particle nucleation turned out to be relevant as well (Table 1 and Fig. 3a). Thus, injecting aqueous $AgNO_3$ at 0 °C results in β-Ag_2MoO_4 cubes (Fig. 3b), whereas β-Ag_2MoO_4 cuboctahedra were formed after $AgNO_3$ injection at 50 °C (Fig. 3c). Thereof, the cubes expose {100} crystal facets only, whereas the cuboctahedra show mixed {100} and {111} crystal facets. Again, the β-Ag_2MoO_4 microcrystals are colorless and do not show any plasmon-resonance absorption (Table 1 and Fig. 3d, compare Fig. 5b), and they also do not show Ag(0)-related spots on electron-microscopy images (Fig. 3b,c) if the exposition under the electron beam was not too long (Fig. 4).

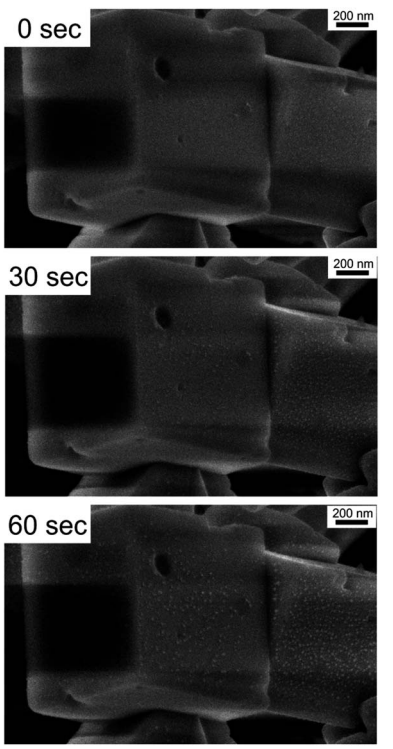

Fig. 4 Evolution of Ag(0)-related spots, up to 10 ± 4 nm in diameter, due to electron-beam-driven reduction on the surface of β-Ag_2MoO_4 cubes after 60 seconds.

Crystallinity and optical properties

All faceted β-Ag_2MoO_4 microcrystals – independent of their respective synthesis in DEG or DMSO – are highly crystalline (Fig. 5a). X-ray powder diffraction (XRD) displays all characteristic Bragg peaks of β-Ag_2MoO_4.[17] In fact, this finding is expected since faceted shapes need to be single crystalline for facet formation. The optical properties were characterized by

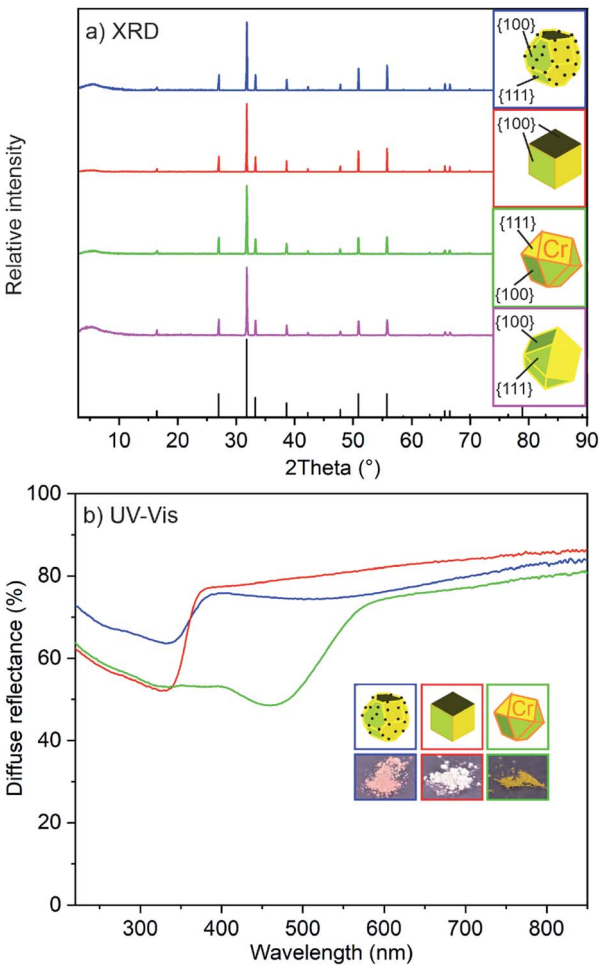

Fig. 5 Crystallinity and optical absorption of the as-prepared β-Ag_2MoO_4 microcrystals: (a) XRD (with bulk β-Ag_2MoO_4, ICSD no. 00-070-1497 as a reference) and (b) UV-Vis spectra of truncated Ag_2MoO_4@Ag octahedra (made in DEG; blue; plasmon-resonance absorption indicated by blue star), Ag_2MoO_4 cubes (made in DMSO; red), Ag_2MoO_4 cuboctahedra (made in DMSO; violet), $Ag_2(Mo_{0.95}Cr_{0.05})O_4$ cuboctahedra (made in DMSO; green) with photos of the respective powder samples.

Table 2 Comparison of the relevant material properties and the photocatalytic activity of the as-prepared β-Ag_2MoO_4 microcrystals

Composition (synthesis)	Morphology with exposed facets	Zeta potential/mV	Specific surface area/$m^2\ g^{-1}$	Band gap/eV	Photo-catalytic activity
Ag_2MoO_4@Ag (DEG)	Truncated octahedra {111} + {100}	−43	1	3.0	Poor
Ag_2MoO_4 (DMSO)	Cubes {100}	−37	2	3.2	Medium
Ag_2MoO_4 (DMSO)	Cuboctahedra {111} + {100}	−33	1	3.2	High
$Ag_2(Mo,Cr)O_4$ (DMSO)	Cuboctahedra {111} + {100}	−35	1	2.1	Medium

UV-Vis spectroscopy. Accordingly, the β-Ag_2MoO_4 samples show a steep absorption edge between 330 and 370 nm (Fig. 5b), which can be related to the valence band-to-transition band excitation. Based on Tauc plots, the absorption of DMSO-made β-Ag_2MoO_4 can be ascribed to a direct band gap with an energy of 3.2 eV, which is well in agreement with literature data (3.14 eV).[8] For the DEG-made β-Ag_2MoO_4, the band gap is slightly reduced to 3.0 eV. In contrast to β-Ag_2MoO_4 made in DMSO, moreover, those samples prepared in DEG show a weak and broad plasmon-resonance absorption at 420 to 750 nm due to the presence of Ag(0) nanoparticles (Fig. 5b). In regard of photocatalysis, these β-Ag_2MoO_4@Ag microcrystals can be promising in terms of visible-light absorption as already outlined by Li *et al.*[11d]

Despite of a potential plasmon-resonance-driven visible-light absorption of β-Ag_2MoO_4@Ag, we intended to evaluate other options to enable β-Ag_2MoO_4 for visible-light absorption in absence of Ag(0) nanoparticles. To this concern, partial substitution of $[MoO_4]^{2-}$ by $[CrO_4]^{2-}$ seemed promising. On the one hand, $[CrO_4]^{2-}$ is known for its bright yellow to orange color indicating light absorption in the blue spectral regime. Moreover, both complex anions are of similar size as indicated by solid solution series $Ag_2(Cr,Mo)O_4$ with complete substitution of $[MoO_4]^{2-}$ by $[CrO_4]^{2-}$ and *vice versa*.[18] On the other hand, the blue-light absorption of $[CrO_4]^{2-}$ relates to a ligand-to-metal charge-transfer (LMCT) of a finite complex anion, which – in the case of partial substitution – is not necessarily affecting the band gap of the infinite lattice of the molybdate. Pure Ag_2CrO_4, finally, was reported to have a reddish black color, which is less optimal for photocatalytic application.[11b]

As a result of the aforementioned considerations, we intended a substitution of 5 mol% of chromate in β-Ag_2MoO_4. $Ag_2(Mo_{0.95}Cr_{0.05})O_4$ was prepared similar to β-Ag_2MoO_4 and, for instance, results in cuboctahedra with similar size and shape as observed for pure β-Ag_2MoO_4. In contrast to colorless β-Ag_2MoO_4, $Ag_2(Mo_{0.95}Cr_{0.05})O_4$ indeed exhibits a bright yellow color (Fig. 5b). UV-Vis spectra show a steep absorption for $Ag_2(Mo_{0.95}Cr_{0.05})O_4$, which is now red-shifted (470–570 nm) in comparison to the β-Ag_2MoO_4 cuboctahedra (Fig. 5b). The band gap of $Ag_2(Mo_{0.95}Cr_{0.05})O_4$ was deduced to 2.1 eV, which lays in between of the values of β-Ag_2MoO_4 (3.14 eV)[18] and Ag_2CrO_4 (1.75 eV).[11b,19] This finding points to an active role of chromate for the band gap of $Ag_2(Mo_{0.95}Cr_{0.05})O_4$.

Photocatalytic examination

For a comparative evaluation of the photocatalytic activity of the different β-Ag_2MoO_4 microcrystals in dependence of their respective surface faceting and chemical composition, the respective experiments were performed with comparable conditions. Thus, identical concentrations of the respective β-Ag_2MoO_4 microcrystals (0.18 g L^{-1}) were suspended in water, and identical concentrations of zwitterionic rhodamine B (RhB, 2 mg L^{-1}, 4.18 μmol L^{-1}) were added. RhB was selected, on the one hand, since its absorption (500–600 nm) is different from the absorption of β-Ag_2MoO_4 (<500 nm). On the other hand, the adhesion of the zwitterionic RhB on the photocatalyst surface is independent from eventual charging of the respective surface of the photocatalyst. Additional criteria for the photocatalytic performance of the β-Ag_2MoO_4 microcrystals were examined as well (Table 2). First of all, the crystallinity and size of the β-Ag_2MoO_4 microcrystals (about 0.5 μm) can be considered as very comparable. Nitrogen sorption analysis also indicated the specific surface area to be similar (Table 2). Finally, the zeta potential was quantified to evaluate a potential influence of surface charging. As a result, all β-Ag_2MoO_4 microcrystals show negative charging ranging from −33 to −43 mV at pH = 7 (Table 2). Finally, any photoluminescence as potential competitive loss process to photoluminescence could be excluded (ESI: Fig. S1†). Taken together, several material parameters – including concentrations, size, crystallinity, surface area and surface charging – are similar, so that a direct correlation of the photocatalytic activity to the type of surface faceting and chemical composition is possible.

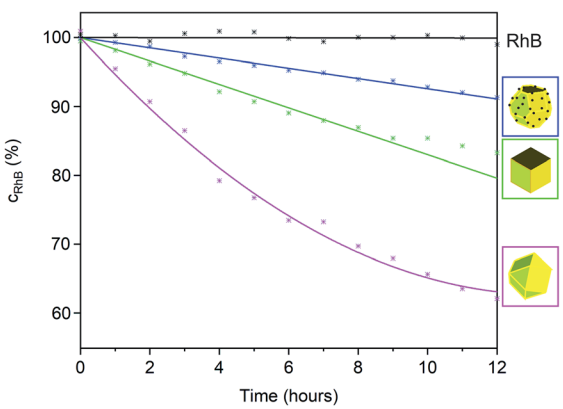

Fig. 6 Photocatalytic evaluation of β-Ag_2MoO_4 cuboctahedra and cubes as well as truncated β-Ag_2MoO_4@Ag octahedra depending on the type of surface facets (c_0(RhB): 0.18 g L^{-1}; c(β-Ag_2MoO_4): 0.20 mg L^{-1}; autophotolysis of RhB as a reference, illumination with simulated sunlight; every tenth raw data point shown).

To examine the photocatalytic activity of the β-Ag_2MoO_4 microcrystals, the absorption of RhB was continuously monitored at $\lambda_{RhB} = 554$ nm under artificial sunlight (AM 1.5 G solar light, 100 mW cm^{-2}) (Fig. 6 and 7). First of all, the autophotolysis of RhB (in absence of β-Ag_2MoO_4) was verified and showed no considerable effect within the significance of the experiment. Thereafter, the different β-Ag_2MoO_4 microcrystals were studied and evidence a significantly higher photocatalytic activity as compared to the autophotolysis of RhB. It should also be noticed that the size and shape of the faceted microcrystals was maintained subsequent to the photocatalytic reaction (ESI: Fig. S2†).

With simulated sunlight, the β-Ag_2MoO_4 cuboctahedra made in DMSO show the highest photocatalytic activity, which is about twice to thrice as high as for all other faceted microcrystals (Fig. 6). The β-Ag_2MoO_4@Ag truncated octahedra made in DEG show the lowest activity, followed by β-Ag_2MoO_4 cubes made in DMSO. In regard of the surface faceting, the photocatalytic activity of {111} crystal facets is obviously higher as compared to {100} crystal facets (Fig. 6). Such situation is well known for metal oxides such as Cu_2O, γ-Al_2O_3 or Co_3O_4 and was related to the higher surface energy of the {111} crystal facets.[20] Since cubes exhibit only {100} facets, they show the lowest photocatalytic activity. The β-Ag_2MoO_4 cuboctahedra, having the highest area of {111} crystal facets, consequently exhibit the highest photocatalytic activity.

Whereas the aforementioned β-Ag_2MoO_4 cubes and cuboctahedra only become photoactive upon absorption of UV photons (<390 nm due to a band gap at 3.2 eV), the truncated β-Ag_2MoO_4@Ag octahedra and $Ag_2(Mo_{0.95}Cr_{0.05})O_4$ cuboctahedra are suitable for visible-light-driven photocatalysis, in principle. However, β-Ag_2MoO_4@Ag already under simulated sunlight with high-energy UV photons absorbed by β-Ag_2MoO_4@Ag shows low performance (Fig. 6). The low activity of β-Ag_2MoO_4@Ag that we observed is in contrast to former studies suggesting a considerable effect of Ag(0) particles on the photocatalytic activity of β-Ag_2MoO_4, which was claimed to be driven by plasmon-resonance absorption even at low wavelength (<420 nm)[11d] or with significantly larger Ag(0) nanoparticles (80–100 nm).[21] Due to its low performance, β-Ag_2MoO_4@Ag was not examined further in our study.

A comparison of the β-Ag_2MoO_4 cuboctahedra as the most active photocatalyst under simulated sunlight (Fig. 6 and 7) and the $Ag_2(Mo_{0.95}Cr_{0.05})O_4$ cuboctahedra (Fig. 7), finally, shows an increased relative photocatalytic activity of $Ag_2(Mo_{0.95}Cr_{0.05})O_4$ the longer the wavelength of the irradiated light is. Thus, illumination only with visible light >400 nm results in a higher photocatalytic activity of the $Ag_2(Mo_{0.95}Cr_{0.05})O_4$ cuboctahedra as compared to the β-Ag_2MoO_4 cuboctahedra (Fig. 7). Such effect of a chromate-shifted optical absorption of a molybdate-based photocatalyst is shown for the first time and offers an additional option for visible-light-driven photocatalysis of metal molybdates and tungstates.

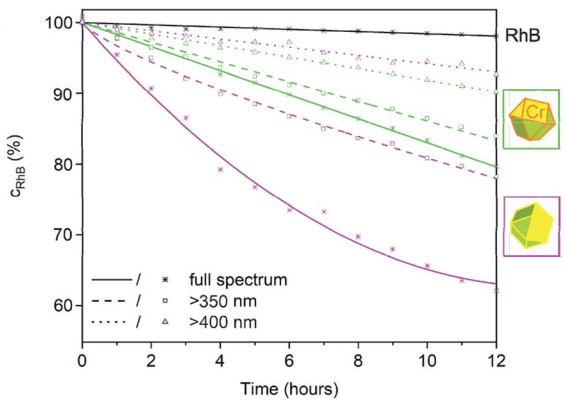

Fig. 7 Photocatalytic evaluation of β-Ag_2MoO_4 and $Ag_2(Mo,Cr)O_4$ cuboctahedra depending on the wavelength of illumination with simulated sunlight as well as with cut-off filters for UV light (cut-off <350/<400 nm, c_0(RhB): 0.18 g L^{-1}; c(β-Ag_2MoO_4): 0.20 mg L^{-1}; autophotolysis of RhB as a reference; every tenth raw data point shown).

Conclusions

Faceted β-Ag_2MoO_4 microcrystals are prepared by controlled nucleation and growth in diethylene glycol (DEG) and dimethylsulfoxide (DMSO). Both serve as solvents for the liquid-phase synthesis and surface-active agents for the formation of faceted microcrystals. Due to the reducing properties, truncated β-Ag_2MoO_4@Ag octahedra are obtained in DEG. The synthesis in DMSO allows avoiding the formation of elemental silver and results in β-Ag_2MoO_4 cubes and cuboctahedra. Whereas the colorless β-Ag_2MoO_4 (band gap: 3.2 eV) can be only activated by UV-light, β-Ag_2MoO_4@Ag (with Ag(0)-based plasmon-resonance absorption) as well as β-$Ag_2(Mo_{0.95}Cr_{0.05})O_4$ (with partial substitution of $[MoO_4]^{2-}$ by $[CrO_4]^{2-}$) are suitable for visible-light excitation.

Based on the realized faceting and chemical composition – truncated octahedra, cubes, cuboctahedra, β-Ag_2MoO_4, β-Ag_2MoO_4@Ag, β-$Ag_2(Mo_{0.95}Cr_{0.05})O_4$ – the photocatalytic properties were exemplarily monitored for the degradation of rhodamine B. As a result, the β-Ag_2MoO_4 cuboctahedra showed the highest photocatalytic activity under simulated sunlight, which could be related to their {111} crystal facets that turned out to be more active than {100} crystal facets. β-Ag_2MoO_4@Ag showed the lowest photocatalytical activity at all. The photocatalytic activity of $Ag_2(Mo_{0.95}Cr_{0.05})O_4$ cuboctahedra turned out to be the higher in comparison to β-Ag_2MoO_4 cuboctahedra the longer the wavelength of the irradiated light is. The facet-, composition- and wavelength-depending photocatalytic activity generally contributes to the fundamental understanding of photocatalysis. The partial incorporation of chromate into molybdate-based photocatalysts and the resulting shift of the optical absorption are shown for the first time and can be of general interest for visible-light-driven photocatalysis of metal molybdates and tungstates.

Conflicts of interest

There are no conflicts to declare.

Acknowledgements

The authors thank the Deutsche Forschungsgemeinschaft (DFG) for funding of equipment. Moreover, L. W. acknowledges the Studienstiftung des deutschen Volkes for scholarship.

Notes and references

1 (*a*) L. Han, S. Cai, M. Gao, J. Hasegawa, P. Wang, J. Zhang, L. Shi and D. Zhang, *Chem. Rev.*, 2019, **119**, 10916–10976; (*b*) A. M. Kaczmarek and R. van Deun, *Chem. Soc. Rev.*, 2013, **42**, 8835–8848.

2 (*a*) H. S. Kim, J. B. Cook, H. Lin, J. S. Ko, S. H. Tolbert, V. Ozolins and B. Dunn, *Nat. Mater.*, 2017, **16**, 454–460; (*b*) X. Hu, W. Zhang, X. Liu, Y. Mei and Y. Huang, *Chem. Soc. Rev.*, 2015, **44**, 2376–2404; (*c*) C. Wang, L. Wu, H. Wang, W. Zuo, Y. Li and J. Liu, *Adv. Funct. Mater.*, 2015, **25**, 3524–3533; (*d*) R. Wu, J. Zhang, Y. Shi, D. Liu and B. Zhang, *J. Am. Chem. Soc.*, 2015, **137**, 6983–6986.

3 (*a*) T. Guo, Y. Lin, W. J. Zhang, J. S. Hong, R. H. Lin, X. P. Wu, J. Li, C. H. Lu and H. H. Yang, *Nanoscale*, 2018, **10**, 1607–1612; (*b*) W. Ouyang, *Small*, 2017, **13**, 2177; (*c*) W. Wang, J. Qin, Z. Yin and M. Cao, *ACS Nano*, 2016, **10**, 10106–10116; (*d*) J. Han, C. McBean, L. Wang, J. Hoy, C. Jaye, H. Liu, Z. Q. Li, M. Y. Sfeir, D. A. Fischer and G. T. Taylor, *Chem. Mater.*, 2015, **27**, 778–792; (*e*) Y. Ma, Y. Jia, Z. Jiao, M. Yang, Y. Qi and Y. Bi, *Chem. Commun.*, 2015, **51**, 6655–6658; (*f*) A. Kudo, M. Steinberg, A. J. Bard, A. Campion, M. A. Fox, T. E. Mallouk, S. E. Webber and J. W. White, *Catal. Lett.*, 1990, **5**, 61–66.

4 (*a*) Y. Park, K. J. Mcdonald and K.-S. Choi, *Chem. Soc. Rev.*, 2013, **42**, 2321–2337; (*b*) A. Walsh, D. J. Payne, R. G. Egdell and G. W. Watson, *Chem. Soc. Rev.*, 2011, **40**, 4455–4463.

5 (*a*) B. Qian, X. Li and Z. Song, *J. Am. Ceram. Soc.*, 2018, **101**, 4425–4429; (*b*) J. Liu, Y. Li, Z. Li, J. Ke, H. Xiao and Y. Hou, *Catal. Today*, 2018, **314**, 2–9; (*c*) A. Etogo, R. Liu, J. Ren, L. Qi, C. Zheng, J. Ning, Y. Zhong and Y. Hu, *J. Mater. Chem. A*, 2016, **4**, 13242–13250.

6 (*a*) D. Mukherjee and B. M. Reddy, *Catal. Today*, 2018, **309**, 227–235; (*b*) H. Y. Kim, M. S. Hybertsen and P. Liu, *Nano Lett.*, 2017, **17**, 348–354; (*c*) A. Trovarelli and J. Llorca, *ACS Catal.*, 2017, **7**, 4716–4735.

7 (*a*) S. K. Meena, N. L. Heda, G. Arora, L. Meena and B. L. Ahuja, *Phys. B*, 2019, **560**, 236–243; (*b*) M. Wu, H. Lv, T. Wang, Z. Ao, H. Sun, C. Wang, T. An and S. Wang, *Catal. Today*, 2018, **315**, 205–212.

8 (*a*) C. A. Oliveira, D. P. Volanti, A. E. Nogueira, C. A. Zamperini, C. E. Vergani and E. Longo, *Mater. Des.*, 2017, **115**, 73–81; (*b*) J. V. Kumar, R. Karthik, S.-M. Chen, V. Muthuraj and C. Karuppiah, *Sci. Rep.*, 2016, **6**, 34149; (*c*) A. Beltrán, L. Gracia, E. Longo and J. Andrés, *J. Phys. Chem. C*, 2014, **118**, 3724–3732.

9 (*a*) R. Kohlmuller and J.-P. Faurie, *Bull. Soc. Chim. Fr.*, 1968, **11**, 4379–4382; (*b*) C. H. B. Ng and W. Y. Fan, *Cryst. Growth Des.*, 2015, **15**, 3032–3037.

10 Z. Wang, K. Dai, C. Liang, J. Zhang and G. Zhu, *Mater. Lett.*, 2017, **196**, 373–376.

11 (*a*) M. T. Fabbro, C. C. Foggi, L. P. S. Santos, L. Gracia, A. Perrin, C. Perrin, C. E. Vergani, A. L. Machado, J. Andrés and E. Cordoncillo, *Dalton Trans.*, 2016, **45**, 10736–10743; (*b*) D. Xu, B. Cheng, J. Zhang, W. Wang, J. Yu and W. Ho, *J. Mater. Chem. A*, 2015, **3**, 20153–20166; (*c*) F. S. Cunha, J. C. Sczancoski, I. C. Nogueira, V. G. de Oliveira, S. M. C. Lustosa, E. Longo and L. S. Cavalcante, *CrystEngComm*, 2015, **17**, 8207–8211; (*d*) A. F. Gouveia, J. C. Sczancoski, M. M. Ferrer, A. S. Lima, M. R. M. C. Santos, M. S. Li, R. S. Santos, E. Longo and L. S. Cavalcante, *Inorg. Chem.*, 2014, **53**, 5589–5599; (*e*) Z. Li, X. Chen and Z.-L. Xue, *Sci. China: Chem.*, 2013, **56**, 443–450.

12 Y.-C. Chen, Y.-K. Hsu, R. Popescu, D. Gerthsen, Y.-G. Lin and C. Feldmann, *Nat. Commun.*, 2018, **9**, 1–11.

13 P. Schmitt, N. Brem, S. Schunk and C. Feldmann, *Adv. Funct. Mater.*, 2011, **21**, 3037–3046.

14 (*a*) Y.-C. Chen, Y.-G. Lin, L.-C. Hsu, A. Tarasov, P.-T. Chen, M. Hayashi, J. Ungelenk, Y.-K. Hsu and C. Feldmann, *ACS Catal.*, 2016, **6**, 2357–2367; (*b*) J. Ungelenk and C. Feldmann, *Chem. Commun.*, 2012, **48**, 7838–7840.

15 H. Dong, Y.-C. Chen and C. Feldmann, *Green Chem.*, 2015, **17**, 4107–4132.

16 (*a*) M. Rycenga, C. M. Cobley, J. Zeng, W. Li, C. H. Moran, Q. Zhang, D. Qin and Y. Xia, *Chem. Rev.*, 2011, **111**, 3669–3712; (*b*) B. D. Evanoff and G. Chumanov, *J. Phys. Chem. B*, 2004, **108**, 13957–13962.

17 R. W. G. Wyckoff, *J. Am. Chem. Soc.*, 1922, **44**, 1994–1998.

18 M. L. Hackert and R. A. Jacobson, *J. Solid State Chem.*, 1971, **3**, 364–368.

19 S. Ouyang, Z. Li, Z. Ouyang, T. Yu, J. Ye and Z. Zou, *J. Phys. Chem. C*, 2008, **112**, 3134–3141.

20 (*a*) Y.-Y. Song and G.-C. Wang, *J. Phys. Chem. C*, 2018, **122**, 21500–21513; (*b*) Y. Wang, J. Yang, R. Gu, L. Peng, X. Guo, N. Xue, Y. Zhu and W. Ding, *ACS Catal.*, 2018, **8**, 6419–6425; (*c*) L. Liu, Z. Jiang, L. Fang, H. Xu, H. Zhang, X. Gu and Y. Wang, *ACS Appl. Mater. Interfaces*, 2017, **9**, 27736–27744.

21 J. Li, F. Liu and Y. Li, *New J. Chem.*, 2018, **42**, 12054–12061.